

An effective all-atom potential for proteins

Anders Irbäck¹, Simon Mitternacht¹ and Sandipan Mohanty²

¹ Computational Biology & Biological Physics, Department of Theoretical Physics, Lund University, Sölvegatan 14A, SE-223 62 Lund, Sweden ²Jülich Supercomputing Center, Institute for Advanced Simulation, Forschungszentrum Jülich, Germany

PMC Biophysics 2009, 2:2

We describe and test an implicit solvent all-atom potential for simulations of protein folding and aggregation. The potential is developed through studies of structural and thermodynamic properties of 17 peptides with diverse secondary structure. Results obtained using the final form of the potential are presented for all these peptides. The same model, with unchanged parameters, is furthermore applied to a heterodimeric coiled-coil system, a mixed α/β protein and a three-helix-bundle protein, with very good results. The computational efficiency of the potential makes it possible to investigate the free-energy landscape of these 49–67-residue systems with high statistical accuracy, using only modest computational resources by today's standards.

INTRODUCTION

A molecular understanding of living systems requires modeling of the dynamics and interactions of proteins. The relevant dynamics of a protein may amount to small fluctuations about its native structure, or reorientations of its ordered parts relative to each other. In either case, a tiny fraction of the conformational space is explored. For flexible proteins, perhaps with large intrinsically disordered parts (1; 2), the situation is different. When studying such proteins or conformational conversion processes like folding or amyloid aggregation, the competition between different minima on the free-energy landscape inevitably comes into focus. Studying these systems by computer simulation is a challenge, because proper sampling of all relevant free-energy minima must be ensured. This goal is very hard to achieve if explicit solvent molecules are included in the

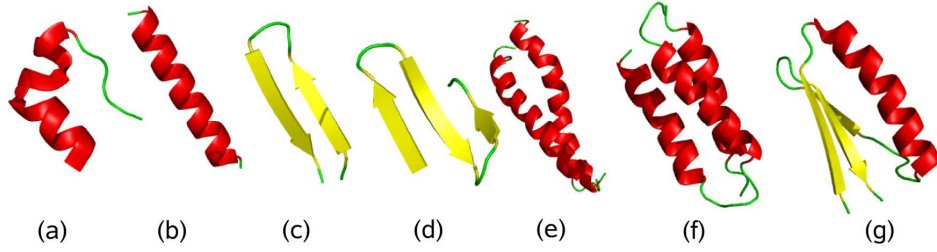


Figure 1: Schematic illustration of native geometries studied. (a) the Trp-cage, (b) an α -helix, (c) a β -hairpin, (d) a three-stranded β -sheet, (e) an α -helix dimer (1U2U), (f) a three-helix bundle (1LQ7), and (g) a mixed α/β protein (2GJH).

simulations. The use of coarse-grained models can alleviate this problem, but makes important geometric properties like secondary structure formation more difficult to describe.

Here we present an implicit solvent all-atom protein model especially aimed at problems requiring exploration of the global free-energy landscape. It is based on a computationally convenient effective potential, with parameters determined through full-scale thermodynamic simulations of a set of experimentally well characterized peptides. Central to the approach is the use of a single set of model parameters, independent of the protein studied. This constraint is a simple but efficient way to avoid unphysical biases, for example, toward either α -helical or β -sheet structure (3; 4). Imposing this constraint is also a way to enable systematic refinement of the potential.

An earlier version (5; 6) of this potential has proven useful, for example, for studies of aggregation (7; 8; 9) and mechanical unfolding (10; 11). Also, using a slightly modified form of the potential (12), the folding mechanisms of a 49-residue protein, Top7-CFr, were investigated (13; 14). Here we revise this potential, through studies of an enlarged set of 17 peptides (see Table 1 and Figure 0). We show that the model, in its final form, folds these different sequences to structures similar to their experimental structures, using a single set of potential parameters. The description of each peptide is kept brief, to be able to discuss all systems and thereby address the issue of transferability in a direct manner. The main purpose of this study is model development rather than detailed characterization of individual systems.

Whether or not this potential, calibrated using data on peptides with typically ~ 20 residues, will be useful for larger systems is not obvious. Therefore, we also apply our potential, with unchanged parameters, to three larger systems with dif-

Table 1: Amino acid sequences. Suc stands for succinyllic acid.

System	PDB code	Sequence
Trp-cage	1L2Y	NLYIQ WLKDG GPSSG RPPPS
E6apn1	1RIJ	Ac-ALQEL LGQWL KDGGP SSGRP PPS-NH ₂
C		Ac-KETAA AKFER AHA-NH ₂
EK		Ac-YAEAA KAAEA AKAF-NH ₂
F _s		Suc-AAAAA AAARA AAARA AAARA A-NH ₂
GCN4tp	2OVN	NYHLE NEVAR LKKLV GE
HPLC-6	1WFA	DTASD AAAAA ALTAA NAKAA AELTA ANAAA AAAAT AR-NH ₂
Chignolin	1UAO	GYDPE TGTWG
MBH12	1J4M	RGKWT YNGIT YEGR
GB1p		GEWTY DDATK TFTVT E
GB1m2		GEWTY NPATG KFTVT E
GB1m3		KKWTY NPATG KFTVQ E
trpzip1	1LE0	SWTWE GNKWT WK-NH ₂
trpzip2	1LE1	SWTWE NGKWT WK-NH ₂
betanova		RGWSV QNGKY TNNGK TTEGR
LLM		RGWSL QNGKY TLNGK TMEGR
beta3s		TWIQN GSTKW YQNGS TKIYT
AB zipper	1U2U	Ac-EVAQL EKEVA QLEAE NYQLE QEVAQ LEHEG-NH ₂ Ac-EVQAL KKRQV ALKAR NYALK QKVQA LRHKG-NH ₂
Top7-CFR	2GJH	ERVRI SITAR TKKEA EKFAA ILIKV FAELG YNDIN VTWDG DTVTV EGQL
GS- α_3 W	1LQ7	GSRVK ALEEK VKALE EKVKA LGGGG RIEEL KKKWE ELKKK IEELG GGGEV KKVVE EVKKL EEEIK KL

ferent geometries. These systems are the mixed α/β protein Top7-CFr, a three-helix-bundle protein with 67 residues, and a heterodimeric leucine zipper composed of two 30-residue chains.

Protein folding simulations are by necessity based on potentials whose terms are interdependent and dependent on the choice of geometric representation. Therefore, we choose to calibrate our potential directly against folding properties of whole chains. To make this feasible, we deliberately omit many details included in force fields like Amber, CHARMM and OPLS (for a review, see (15)). With this approach, we might lose details of a given free-energy minimum, but, by construction, we optimize the balance between competing minima.

Two potentials somewhat similar in form to ours are the μ -potential of the Shakhnovich group (16) and the PFF potential of the Wenzel group (17). These groups also consider properties of entire chains for calibration, but use folded PDB structures or sets of decoys rather than full-scale thermodynamic simulations. Our admittedly time-consuming procedure implies that our model is trained on completely general structures, which might be an advantage when studying the dynamics of folding. Another potential with similarities to ours is that developed by the Dokholyan group for discrete molecular dynamics simulations (18).

METHODS

Our model belongs to the class of implicit solvent all-atom models with torsional degrees of freedom. All geometrical parameters, like bond lengths and bond angles, are as described earlier (5).

The interaction potential is composed of four major terms:

$$E = E_{\text{loc}} + E_{\text{ev}} + E_{\text{hb}} + E_{\text{sc}}. \quad (1)$$

The first term, E_{loc} , contains local interactions between atoms separated by only a few covalent bonds. The other three terms are non-local in character: E_{ev} represents excluded-volume effects, E_{hb} is a hydrogen-bond potential, and E_{sc} contains residue-specific interactions between pairs of side-chains. Next we describe the precise form of these four terms. Energy parameters are given in a unit called eu. The factor for conversion from eu to kcal/mol will be determined in the next section, by calibration against the experimental melting temperature for one of the peptides studied, the Trp-cage.

Local potential. The local potential $E_{\text{loc}} = E_{\text{loc}}^{(1)} + E_{\text{loc}}^{(2)} + E_{\text{loc}}^{(3)}$ can be divided into two backbone terms, $E_{\text{loc}}^{(1)}$ and $E_{\text{loc}}^{(2)}$, and one side-chain term, $E_{\text{loc}}^{(3)}$. In describing the potential, the concept of a peptide unit is useful. A peptide unit consists of the backbone C'O group of one residue and the backbone NH group of the next residue.

- The potential $E_{\text{loc}}^{(1)}$ represents interactions between partial charges of neighboring peptide units along the chain. It is given by

$$E_{\text{loc}}^{(1)} = \kappa_{\text{loc}}^{(1)} \sum_{\text{n.n.}} \sum_i \sum_j \frac{q_i q_j}{r_{ij}/\text{\AA}}, \quad (2)$$

where the outer sum runs over all pairs of nearest-neighbor peptide units and each of the two inner sums runs over atoms in one peptide unit (if the N side of the peptide unit is proline the sum runs over only C' and O). The partial charge q_i is taken as ± 0.42 for C' and O atoms and ± 0.20 for H and N atoms. The parameter $\kappa_{\text{loc}}^{(1)}$ is set to 6 eu, corresponding to a dielectric constant of $\epsilon_r \approx 41$. Two peptide units that are not nearest neighbors along the chain interact through hydrogen bonding (see below) rather than through the potential $E_{\text{loc}}^{(1)}$.

- The term $E_{\text{loc}}^{(2)}$ provides an additional OO and HH repulsion for neighboring peptide units, unless the residue flanked by the two peptide units is a glycine. This repulsion is added to make doubling of hydrogen bonds less likely. Glycine has markedly different backbone energetics compared to other residues. The lack of C_β atom makes glycine more flexible. However, the observed distribution of Ramachandran ϕ, ψ angles for glycine in PDB structures (19) is not as broad as simple steric considerations would suggest. $E_{\text{loc}}^{(2)}$ provides an energy penalty for glycine ψ values around $\pm 120^\circ$, which are sterically allowed but relatively rare in PDB structures.

The full expression for $E_{\text{loc}}^{(2)}$ is

$$E_{\text{loc}}^{(2)} = \kappa_{\text{loc}}^{(2)} \sum_{\text{non-Gly}} [f(u_I) + f(v_I)] + \kappa_{\text{loc,G}}^{(2)} \sum_{\text{Gly}} (\cos \psi_I + 2 \cos 2\psi_I), \quad (3)$$

where $\kappa_{\text{loc}}^{(2)} = 1.2$ eu, $\kappa_{\text{loc,G}}^{(2)} = -0.15$ eu, I is a residue index, and

$$u_I = \min[d(\text{H}_I, \text{N}_{I+1}), d(\text{N}_I, \text{H}_{I+1})] - d(\text{H}_I, \text{H}_{I+1}) \quad (4)$$

$$v_I = \min[d(\text{O}_I, \text{C}'_{I+1}), d(\text{C}'_I, \text{O}_{I+1})] - d(\text{O}_I, \text{O}_{I+1}) \quad (5)$$

$$f(x) = \max(0, \tanh 3x) \quad (6)$$

Table 2: Classification of side-chain angles, χ_i . The parameters of the torsion angle potential $E_{\text{loc}}^{(3)}$ are $(\kappa_{\text{loc},i}^{(3)}, n_i) = (0.6 \text{ eu}, 3)$ for class I, $(\kappa_{\text{loc},i}^{(3)}, n_i) = (0.3 \text{ eu}, 3)$ for class II, $(\kappa_{\text{loc},i}^{(3)}, n_i) = (0.4 \text{ eu}, 2)$ for class III, and $(\kappa_{\text{loc},i}^{(3)}, n_i) = (-0.4 \text{ eu}, 2)$ for class IV.

Residue	χ_1	χ_2	χ_3	χ_4
Ser, Cys, Thr, Val	I			
Ile, Leu	I	I		
Asp, Asn	I	IV		
His, Phe, Tyr, Trp	I	III		
Met	I	I	II	
Glu, Gln	I	I	IV	
Lys	I	I	I	I
Arg	I	I	I	III

The function $f(u_I)$ is positive if the $H_I H_{I+1}$ distance, $d(H_I, H_{I+1})$, is smaller than both of the $H_I N_{I+1}$ and $N_I H_{I+1}$ distances, and zero otherwise. This term thus provides an energy penalty when H_I and H_{I+1} are exposed to each other (it is omitted if residue I or $I + 1$ is a proline). Similarly, $f(v_I)$ is positive when O_I and O_{I+1} are exposed to each other.

- $E_{\text{loc}}^{(3)}$ is an explicit torsion angle potential for side-chain angles, χ_i . Many side-chain angles display distributions resembling what one would expect based on simple steric considerations. The use of the torsion potential is particularly relevant for χ_2 in asparagine and aspartic acid and χ_3 in glutamine and glutamic acid. The torsion potential is defined as

$$E_{\text{loc}}^{(3)} = \sum_i \kappa_{\text{loc},i}^{(3)} \cos n_i \chi_i, \quad (7)$$

where $\kappa_{\text{loc},i}^{(3)}$ and n_i are constants. Each side-chain angle χ_i belongs to one of four classes associated with different values of $\kappa_{\text{loc},i}^{(3)}$ and n_i (see Table 2).

Excluded volume. Excluded-volume effects are modeled using the potential

$$E_{\text{ev}} = \kappa_{\text{ev}} \sum_{i < j} \left[\frac{\lambda_{ij}(\sigma_i + \sigma_j)}{r_{ij}} \right]^{12}, \quad (8)$$

where the summation is over all pairs of atoms with a non-constant separation, $\kappa_{\text{ev}} = 0.10 \text{ eu}$, and $\sigma_i = 1.77, 1.75, 1.53, 1.42$ and 1.00 \AA for S, C, N, O and H atoms,

respectively. The parameter λ_{ij} is unity for pairs connected by three covalent bonds and $\lambda_{ij}=0.75$ for all other pairs. To speed up the calculations, E_{ev} is evaluated using a cutoff of $4.3\lambda_{ij}$ Å.

Hydrogen bonding. Our potential contains an explicit hydrogen-bond term, E_{hb} . All hydrogen bonds in the model are between NH and CO groups. They connect either two backbone groups or a charged side-chain (aspartic acid, glutamic acid, lysine, arginine) with a backbone group. Two neighboring peptide units, which interact through the local potential (see above), are not allowed to hydrogen bond with each other.

The form of the hydrogen-bond potential is

$$E_{hb} = \epsilon_{hb}^{(1)} \sum_{bb-bb} u(r_{ij})v(\alpha_{ij}, \beta_{ij}) + \epsilon_{hb}^{(2)} \sum_{sc-bb} u(r_{ij})v(\alpha_{ij}, \beta_{ij}), \quad (9)$$

where $\epsilon_{hb}^{(1)}=3.0$ eu and $\epsilon_{hb}^{(2)}=2.3$ eu set the strengths of backbone-backbone and sidechain-backbone bonds, respectively, r_{ij} is the HO distance, α_{ij} is the NHO angle, and β_{ij} is the HOC angle. The functions $u(r)$ and $v(\alpha, \beta)$ are given by

$$u(r) = 5 \left(\frac{\sigma_{hb}}{r} \right)^{12} - 6 \left(\frac{\sigma_{hb}}{r} \right)^{10} \quad (10)$$

$$v(\alpha, \beta) = \begin{cases} (\cos \alpha \cos \beta)^{1/2} & \text{if } \alpha, \beta > 90^\circ \\ 0 & \text{otherwise} \end{cases} \quad (11)$$

where $\sigma_{hb} = 2.0$ Å. A 4.5 Å cutoff is used for $u(r)$.

Side-chain potential. Our side-chain potential is composed of two terms, $E_{sc} = E_{hp} + E_{ch}$. The E_{ch} term represents interactions among side-chain charges. The first and more important term, E_{hp} , is meant to capture the effects of all other relevant interactions, especially effective hydrophobic attraction. For convenience, E_{hp} and E_{ch} have a similar form,

$$E_{hp} = - \sum_{I < J} M_{IJ}^{(hp)} C_{IJ}^{(hp)} \quad E_{ch} = - \sum_{I < J} M_{IJ}^{(ch)} C_{IJ}^{(ch)}. \quad (12)$$

Here the sums run over residue pairs IJ , $C_{IJ}^{(hp)}$ and $C_{IJ}^{(ch)}$ are contact measures that take values between 0 and 1, and $M_{IJ}^{(hp)}$ and $M_{IJ}^{(ch)}$ are energy parameters.

It is assumed that ten of the twenty natural amino acids contribute to E_{hp} , see Table 3. Included among these ten are lysine and arginine, which are charged

Table 3: The parameter m_I of the hydrophobicity potential E_{hp} .

Residue	m_I (eu)
Arg	0.3
Met, Lys	0.4
Val	0.6
Ile, Leu, Pro	0.8
Tyr	1.1
Phe, Trp	1.6

but have large hydrophobic parts. To reduce the number of parameters, the hydrophobic contact energies are taken to be additive, $M_{IJ}^{(\text{hp})} = m_I + m_J$. It is known that the statistically derived Miyazawa-Jernigan contact matrix (20) can be approximately decomposed this way (21). The m_I parameters can be found in Table 3. $M_{IJ}^{(\text{hp})}$ is set to 0 if residues I and J are nearest neighbors along the chain, and is reduced by a factor 2 for next-nearest neighbors.

The residues taken as charged are aspartic acid, glutamic acid, lysine and arginine. The charge-charge contact energy is $-M_{IJ}^{(\text{ch})} = 1.5s_I s_J$ eu, where s_I and s_J are the signs of the charges (± 1).

The contact measure $C_{IJ}^{(\text{hp})}$ is calculated using a predetermined set of atoms for each amino acid, denoted by $A_I^{(\text{hp})}$ (see Table 4). Let n_I be the number of atoms in $A_I^{(\text{hp})}$ and let

$$\Gamma_{IJ}^{(\text{hp})} = \sum_{i \in A_I^{(\text{hp})}} g(\min_{j \in A_J^{(\text{hp})}} r_{ij}^2), \quad (13)$$

where $g(x)$ is unity for $x < (3.7\text{\AA})^2$, vanishes for $x > (4.5\text{\AA})^2$, and varies linearly for intermediate x . The contact measure can then be written as

$$C_{IJ}^{(\text{hp})} = \frac{\min(\gamma_{IJ}(n_I + n_J), \Gamma_{IJ}^{(\text{hp})} + \Gamma_{JI}^{(\text{hp})})}{\gamma_{IJ}(n_I + n_J)}, \quad (14)$$

where γ_{IJ} is either 1 or 0.75. For $\gamma_{IJ} = 1$, $C_{IJ}^{(\text{hp})}$ is, roughly speaking, the fraction of atoms in $A_I^{(\text{hp})}$ and $A_J^{(\text{hp})}$ that are in contact with some atom from the other of the two sets. A reduction to $\gamma_{IJ} = 0.75$ makes it easier to achieve a full contact ($C_{IJ}^{(\text{hp})} = 1$). The value $\gamma_{IJ} = 0.75$ is used for interactions within the group proline, phenylalanine, tyrosine and tryptophan, to make face-to-face stacking of these side-chains less likely. It is also used within the group isoleucine, leucine and valine, because a full contact is otherwise hard to achieve for these pairs. In all other cases, γ_{IJ} is unity.

Table 4: Atoms used in the calculation of the contact measure $C_{IJ}^{(\text{hp})}$.

Residue	Set of atoms (A_I)
Pro	$C_\beta, C_\gamma, C_\delta$
Tyr	$C_\gamma, C_{\delta 1}, C_{\delta 2}, C_{\epsilon 1}, C_{\epsilon 2}, C_\zeta$
Val	$C_\beta, C_{\gamma 1}, C_{\gamma 2}$
Ile	$C_\beta, C_{\gamma 1}, C_{\gamma 2}, C_\delta$
Leu	$C_\beta, C_\gamma, C_{\delta 1}, C_{\delta 2}$
Met	$C_\beta, C_\gamma, S_\delta, C_\epsilon$
Phe	$C_\gamma, C_{\delta 1}, C_{\delta 2}, C_{\epsilon 1}, C_{\epsilon 2}, C_\zeta$
Trp	$C_\gamma, C_{\delta 1}, C_{\delta 2}, C_{\epsilon 3}, C_{\zeta 3}, C_{\eta 2}$
Arg	C_β, C_γ
Lys	$C_\beta, C_\gamma, C_\delta$

Table 5: Atoms used in the calculation of the contact measure $C_{IJ}^{(\text{ch})}$.

Residue	Set of atoms (A_I)
Arg	$N_\epsilon, C_\zeta, N_{\eta 1}, N_{\eta 2}$
Lys	$^1H_\zeta, ^2H_\zeta, ^3H_\zeta$
Asp	$O_{\delta 1}, O_{\delta 2}$
Glu	$O_{\epsilon 1}, O_{\epsilon 2}$

The definition of $C_{IJ}^{(\text{ch})}$ is similar. The γ_{IJ} parameter is unity for charge-charge interactions, and the sets of atoms used, $A_I^{(\text{ch})}$, can be found in Table 5.

Chain ends. Some of the sequences we study have extra groups attached at one or both ends of the chain. The groups occurring are N-terminal acetyl and succinyl acid, and C-terminal NH_2 . When such a unit is present, the model assumes polar NH and CO groups beyond the last C_α atom to hydrogen bond like backbone NH/CO groups but with the strength reduced by a factor 2 (multiplicatively). The charged group of succinyl acid interacts like a charged side-chain.

In the absence of end groups, the model assumes the N and C termini to be positively and negatively charged, respectively, and to interact like charged side-chains.

Monte Carlo details. We investigate the folding thermodynamics of this model by Monte Carlo (MC) methods. The simulations are done using either simulated

Table 6: Algorithm used and total number of elementary MC steps for all systems studied.

System	Method	MC steps
Trp-cage, E6apn1	ST	$10 \times 1.0 \times 10^9$
C, EK, F _s , GCN4tp	ST	$10 \times 1.0 \times 10^9$
HPLC-6	ST	$10 \times 3.0 \times 10^9$
Chignolin	ST	$10 \times 0.5 \times 10^9$
MBH12	ST	$10 \times 1.0 \times 10^9$
GB1p	ST	$10 \times 2.0 \times 10^9$
GB1m2, GB1m3	ST	$10 \times 1.0 \times 10^9$
trpzip1, trpzip2	ST	$10 \times 1.0 \times 10^9$
betanova, LLM	ST	$10 \times 1.0 \times 10^9$
beta3s	ST	$10 \times 2.0 \times 10^9$
AB zipper	PT	$64 \times 3.0 \times 10^9$
Top7-CFR	PT	$64 \times 2.4 \times 10^9$
GS- α_3 W	PT	$64 \times 3.5 \times 10^9$

tempering (ST) (22; 23) or parallel tempering/replica exchange (PT) (24; 25), both with temperature as a dynamical variable. For small systems we use ST, with seven geometrically distributed temperatures in the range 279 K–367 K. For each system, ten independent ST runs are performed. For our largest systems we use PT with a set of sixteen temperatures, spanning the same interval. Using fourfold multiplexing (26), one run comprising 64 parallel trajectories is performed for each system. The PT temperature distribution is determined by an optimization procedure (26). The length of our different simulations can be found in Table 6.

Three different conformational updates are used in the simulations: single variable updates of side-chain and backbone angles, respectively, and Biased Gaussian Steps (BGS) (27). The BGS move is semi-local and updates up to eight consecutive backbone degrees of freedom in a manner that keeps the ends of the segment approximately fixed. The ratio of side-chain to backbone updates is the same at all temperatures, whereas the relative frequency of the two backbone updates depends on the temperature. At high temperatures the single variable update is the only backbone update used, and at low temperatures only BGS is used. At intermediate temperatures both updates are used.

The AB zipper, a two-chain system, is studied using a periodic box of size $(158\text{\AA})^3$. In addition to the conformational updates described above, the sim-

ulations of this system used rigid body translations and rotations of individual chains.

Our simulations are performed using the open source C++-package PROFASI (28). Future public releases of PROFASI will include an implementation of the force field described here. While this force field has been implemented in PROFASI in an optimized manner, this optimization does not involve a parallel evaluation of the potential on many processors. Therefore, in our simulations the number of processors used is the same as the number of MC trajectories generated. For a typical small peptide, a trajectory of the length as given in Table 6 takes ~ 18 hours to generate on an AMD Opteron processor with ~ 2.0 GHz clock rate. For the largest system studied, GS- α_3 W, the simulations, with a proportionately larger number of MC updates, take ~ 10 days to complete.

Analysis. In our simulations, we monitor a variety of different properties. Three important observables are as follows.

1. α -helix content, h . A residue is defined as helical if its Ramachandran angle pair is in the region $-90^\circ < \phi < -30^\circ$, $-77^\circ < \psi < -17^\circ$. Following (29), a stretch of $n > 2$ helical residues is said to form a helical segment of length $n - 2$. For an end residue that is not followed by an extra end group, the (ϕ, ψ) pair is poorly defined. Thus, for a chain with N residues, the maximum length of a helical segment is $N - 4$, $N - 3$ or $N - 2$, depending on whether there are zero, one or two end groups. The α -helix content h is defined as the total length of all helical segments divided by this maximum length.
2. Root-mean-square deviation from a folded reference structure, bRMSD/RMSD/pRMSD. bRMSD is calculated over backbone atoms, whereas RMSD is calculated over all heavy atoms. All residues except the two end residues are included in the calculation, unless otherwise stated. For the case of the dimeric AB zipper, the periodic box used for the simulations has to be taken into account. The two chains in the simulation might superficially appear to be far away when they are in fact close, because of periodicity. For this case we evaluate backbone RMSD over atoms taken from both chains in the dimer, and minimize this value with respect to periodic translations. We denote this as pRMSD.

3. Nativeness measure based on hydrogen bonds, q_{hb} . This observable has the value 1 if at most two native backbone-backbone hydrogen bonds are missing, and is 0 otherwise. A hydrogen bond is considered formed if its energy is less than -1.03 eu.

In many cases, it turns out that the temperature dependence of our results can be approximately described in terms of the simple two-state model

$$X(T) = \frac{X_1 + X_2 K(T)}{1 + K(T)} \quad K(T) = \exp \left[\left(\frac{1}{RT} - \frac{1}{RT_m} \right) \Delta E \right] \quad (15)$$

where $X(T)$ is the quantity studied, X_1 and X_2 are the values of X in the two states, and $K(T)$ is the effective equilibrium constant (R is the gas constant). In this first-order form, $K(T)$ contains two parameters: the melting temperature T_m and the energy difference ΔE . The parameters T_m , ΔE , X_1 and X_2 are determined by fitting to data.

Thermal averages and their statistical errors are calculated by using the jack-knife method (30), after discarding the first 20 % of each MC trajectory for thermalization.

Figures of 3D structures were prepared using PyMOL (31).

RESULTS

We study a total of 20 peptide/protein systems, listed in Table 1 (amino acid sequences can be found in this table). Among these, there are 17 smaller systems with 10–37 residues and 3 larger ones with ≥ 49 residues. Many of the smaller systems have been simulated by other groups, in some cases with explicit water (for a review, see (32)). Two of the three larger systems, as far as we know, have not been studied using other force fields. A study of the 67-residue three-helix-bundle protein GS- α_3 W using the ECEPP/3 force field was recently reported (33). The simulations presented here use the same geometric representation and find about a hundred times the number of independent folding events, while consuming much smaller computing resources.

Trp-cage and E6apn1. The Trp-cage is a designed 20-residue miniprotein with a compact helical structure (34). Its NMR-derived native structure (see Figure 0) contains an α -helix and a single turn of 3_{10} -helix (34). The E6apn1 peptide was

designed using the Trp-cage motif as a scaffold, to inhibit the E6 protein of papillomavirus (35). E6apn1 is three residues larger than the Trp-cage but has a similar structure, except that the α -helix is slightly longer (35).

As indicated earlier, we use melting data for the Trp-cage to set the energy scale of the model. For this peptide, several experiments found a similar melting temperature, $T_m \sim 315$ K (34; 36; 37). In our model, the heat capacity of the Trp-cage displays a maximum at $RT = 0.4722 \pm 0.0008$ eu. Our energy unit eu is converted to kcal/mol by setting this temperature equal to the experimental melting temperature (315 K). Having done that, there is no free parameter left in the model. Other systems are thus studied without tuning any model parameter. For E6apn1, the experimental melting temperature is $T_m \sim 305$ K (35).

Figure 1a shows the helix content h against temperature for the Trp-cage and E6apn1, as obtained from our simulations. In both cases, the T dependence is well described by the simple two-state model of Equation 15. The fitted melting temperatures are $T_m = 309.6 \pm 0.7$ K and $T_m = 304.0 \pm 0.5$ K for the Trp-cage and E6apn1, respectively. This T_m value for the Trp-cage is slightly lower than that we obtain from heat capacity data, 315 K. A fit to our data for the hydrophobicity energy E_{hp} (not shown) gives instead a slightly larger T_m , 321.1 ± 0.8 K. This probe dependence of T_m implies an uncertainty in the determination of the energy scale. By using the Trp-cage, this uncertainty is kept small ($\sim 2\%$). For many other peptides, the spread in T_m is much larger (see below).

Figure 1b shows the free energy calculated as a function of bRMSD for the Trp-cage and E6apn1 at two different temperatures. The first temperature, 279 K, is well below T_m . Here native-like conformations dominate and the global free-energy minima are at 2.4 Å and 2.0 Å for the Trp-cage and E6apn1, respectively. At the second temperature, 306 K, the minima are shifted to higher bRMSD. Note that these free-energy profiles, taken near T_m , show no sign of a double-well structure. Hence, these peptides do not show a genuine two-state behavior in our simulations, even though the melting curves (Figure 1a) are well described by a two-state model, as are many experimentally observed melting curves.

The α -helices C, EK, F_s, GCN4tp and HPLC-6. Our next five sequences form α -helices. Among these, there are large differences in helix stability, according to CD studies. The least stable are the C (38) and EK (39) peptides, which are only partially stable at $T \sim 273$ K. The original C peptide is a 13-residue fragment of ribonuclease A, but the C peptide here is an analogue with two alanine substi-

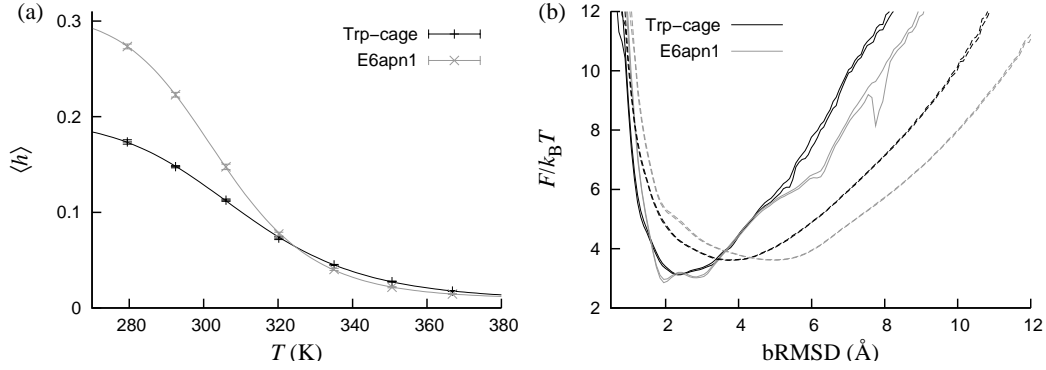


Figure 2: The Trp-cage and E6apn1. (a) Helix content h against temperature. The lines are two-state fits ($T_m = 309.6 \pm 0.7$ K and $\Delta E = 11.3 \pm 0.3$ kcal/mol for the Trp-cage; $T_m = 304.0 \pm 0.5$ K and $\Delta E = 14.2 \pm 0.3$ kcal/mol for E6apn1). (b) Free energy F calculated as a function of bRMSD at two different temperatures, 279 K (solid lines) and 306 K (dashed lines). The double lines indicate the statistical errors.

tutions and a slightly increased helix stability (40). The EK peptide is a designed alanine-based peptide with 14 residues.

Our third α -helix peptide is the 21-residue F_s (41), which is also alanine-based. F_s is more stable than C and EK (41; 42), with estimated T_m values of 308 K (42) and 303 K (43) from CD studies and 334 K from an IR study (44). Even more stable is HPLC-6, a winter flounder antifreeze peptide with 37 residues. CD data suggest that the helix content of HPLC-6 remains non-negligible, ~ 0.10 , at temperatures as high as ~ 343 K (45). Our fifth helix-forming sequence, which we call GCN4tp, has 17 residues and is taken from a study of GCN4 coiled-coil formation (46). Its melting behavior has not been studied, as far as we know, but its structure was characterized by NMR (46).

These five peptides are indeed α -helical in our model. At 279 K, the calculated helix content h is 0.28 for the C peptide, 0.47 for the EK peptide, and > 0.60 for the other three peptides. Figure 2 shows the temperature dependence of h . By fitting Equation 15 to the data for the three stable sequences, we find melting temperatures of 298.9 ± 0.1 K, 309.2 ± 0.3 K and 323.3 ± 1.2 K for GCN4tp, F_s and HPLC-6, respectively.

For the four peptides whose melting behavior has been studied experimentally, these results are in good agreement with experimental data. In particular, we find that HPLC-6 indeed is more stable than F_s in the model, which in turn

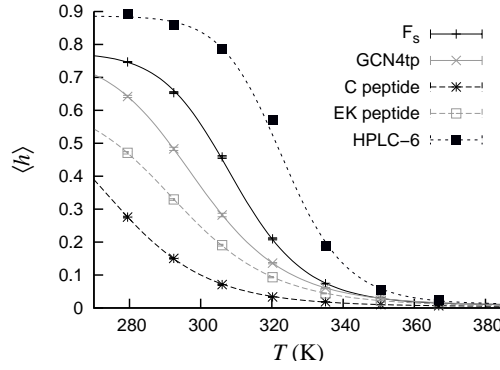


Figure 3: The C, EK, F_s, GCN4tp and HPLC-6 peptides. Helix content h against temperature. The lines are two-state fits ($T_m = 276.3 \pm 2.4$ K and $\Delta E = 11.7 \pm 0.4$ kcal/mol for C; $T_m = 293.9 \pm 0.4$ K and $\Delta E = 12.6 \pm 0.2$ kcal/mol for EK; $T_m = 309.2 \pm 0.3$ K and $\Delta E = 18.7 \pm 0.4$ kcal/mol for F_s; $T_m = 298.9 \pm 0.1$ K and $\Delta E = 14.1 \pm 0.1$ kcal/mol for GCN4tp; $T_m = 323.3 \pm 1.2$ K and $\Delta E = 23.6 \pm 2.2$ kcal/mol for HPLC-6).

is more stable than both C and EK. The model thus captures the stability order among these peptides.

The β -hairpins chignolin and MBH12. We now turn to β -sheet peptides and begin with the β -hairpins chignolin (47) and MBH12 (48) with 10 and 14 residues, respectively. Both are designed and have been characterized by NMR. For chignolin, T_m values in the range 311–315 K were reported (47), based on CD and NMR. We are not aware of any melting data for MBH12.

Figure 3 shows the temperature dependence of the hydrophobicity energy E_{hp} and the nativeness parameter q_{hb} for these peptides. By fitting to E_{hp} data, we obtain $T_m = 311.0 \pm 0.5$ K and $T_m = 315.4 \pm 1.3$ K for chignolin and MBH12, respectively. Using q_{hb} data instead, we find $T_m = 305.4 \pm 0.5$ K for chignolin and $T_m = 309.2 \pm 0.7$ K for MBH12. These T_m values show a significant but relatively weak probe dependence. The values for chignolin can be compared with experimental data, and the agreement is good.

Because these peptides have only four native hydrogen bonds each, one may question our definition of q_{hb} (see Methods), which takes a conformation as native-like ($q_{hb} = 1$) even if two hydrogen bonds are missing. Therefore, we repeated the analysis using the stricter criterion that native-like conformations ($q_{hb} = 1$) may lack at most one hydrogen bond. The resulting decrease in native population, as

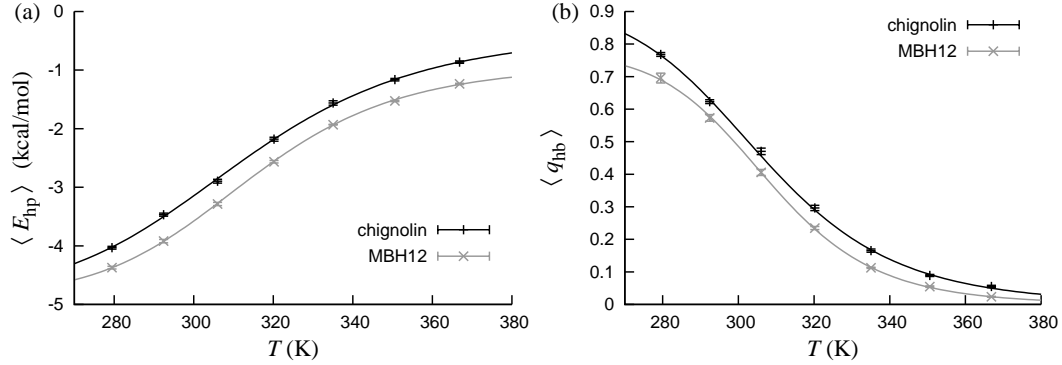


Figure 4: Chignolin and MBH12. (a) Hydrophobicity energy E_{hp} against temperature. The lines are two-state fits ($T_m = 311.0 \pm 0.5$ K and $\Delta E = 9.6 \pm 0.2$ kcal/mol for chignolin; $T_m = 315.4 \pm 1.3$ K and $\Delta E = 9.9 \pm 0.9$ kcal/mol for MBH12). (b) Nativeness q_{hb} against temperature. The lines are two-state fits ($T_m = 305.4 \pm 0.5$ K and $\Delta E = 10.4 \pm 0.1$ kcal/mol for chignolin; $T_m = 309.2 \pm 0.7$ K and $\Delta E = 13.5 \pm 0.2$ kcal/mol for MBH12).

measured by the average q_{hb} , was ~ 0.1 or smaller at all temperatures. Even with this stricter definition, we find native populations well above 0.5 at low temperatures for both peptides.

The β -hairpins GB1p, GB1m2 and GB1m3. GB1p is the second β -hairpin of the B1 domain of protein G (residues 41–56). Its folded population has been estimated by CD/NMR to be 0.42 at 278 K (49) and ~ 0.30 at 298 K (50), whereas a Trp fluorescence study found a T_m of 297 K (51), corresponding to a somewhat higher folded population. GB1m2 and GB1m3 are two mutants of GB1p with significantly enhanced stability (50). At 298 K, the folded population was found to be 0.74 ± 0.05 for GB1m2 and 0.86 ± 0.03 for GB1m3, based on CD and NMR measurements (50). It was further estimated that $T_m = 320 \pm 2$ K for GB1m2 and $T_m = 333 \pm 2$ K for GB1m3 (50).

All these three peptides are believed to adopt a structure similar to that GB1p has as part of the protein G B1 domain (PDB code 1GB1). This part of the full protein contains seven backbone-backbone hydrogen bonds. These hydrogen bonds are the ones we consider when evaluating q_{hb} for these peptides.

Figure 4 shows the observables E_{hp} and q_{hb} against temperature for these peptides. Fits to the data give E_{hp} -based T_m values of 301.7 ± 3.3 K, 324.4 ± 1.1 K and 331.4 ± 0.7 K for GB1p, GB1m2 and GB1m3, respectively, and q_{hb} -based T_m values

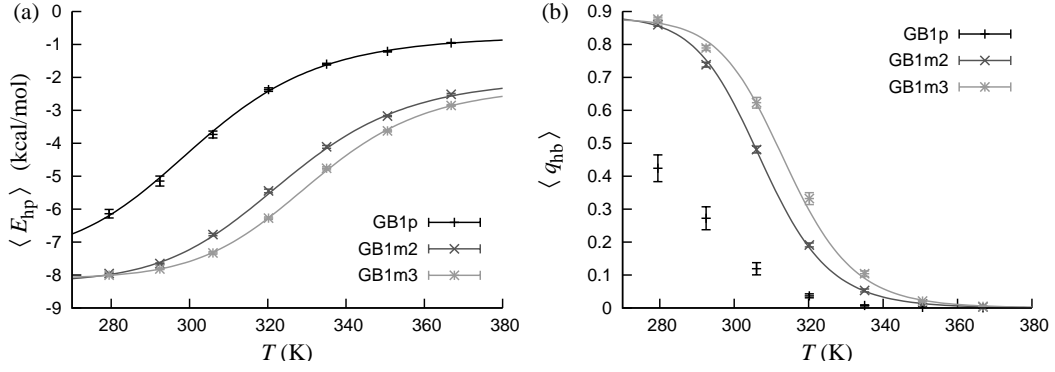


Figure 5: GB1p, GB1m2 and GB1m3. (a) Hydrophobicity energy E_{hp} against temperature. The lines are two-state fits ($T_m = 301.7 \pm 3.3$ K and $\Delta E = 11.3 \pm 1.1$ kcal/mol for GB1p; $T_m = 324.4 \pm 1.4$ K and $\Delta E = 13.2 \pm 1.0$ kcal/mol for GB1m2; $T_m = 331.4 \pm 0.7$ K and $\Delta E = 14.8 \pm 0.5$ kcal/mol for GB1m3). (b) Nativeness q_{hb} against temperature. The lines are two-state fits ($T_m = 307.5 \pm 0.5$ K and $\Delta E = 20.7 \pm 0.5$ kcal/mol for GB1m2; $T_m = 313.9 \pm 1.4$ K and $\Delta E = 21.4 \pm 1.1$ kcal/mol for GB1m3).

of 307.5 ± 0.5 K and 313.9 ± 1.4 K for GB1m2 and GB1m3, respectively. The q_{hb} data do not permit a reliable fit for the less stable GB1p. At 298 K, we find q_{hb} -based folded populations of 0.20, 0.64 and 0.74 for GB1p, GB1m2 and GB1m3, respectively, which can be compared with the above-mentioned experimental results (0.30, 0.74 and 0.86).

These results show that, in the model, the apparent folded populations of these peptides depend quite strongly on the observable studied. Our E_{hp} -based results agree quite well with experimental data, especially for GB1m2 and GB1m3, whereas our q_{hb} results consistently give lower folded populations for all peptides. The stability order is the same independent of which of the two observables we study, namely $GB1p < GB1m2 < GB1m3$, which is the experimentally observed order.

The stability difference between GB1m2 and GB1m3 is mainly due to charge-charge interactions. In our previous model (6), these interactions were ignored, and both peptides had similar stabilities. The present model splits this degeneracy. Moreover, the magnitude of the splitting, which sensitively depends on the strength of the charge-charge interactions, is consistent with experimental data.

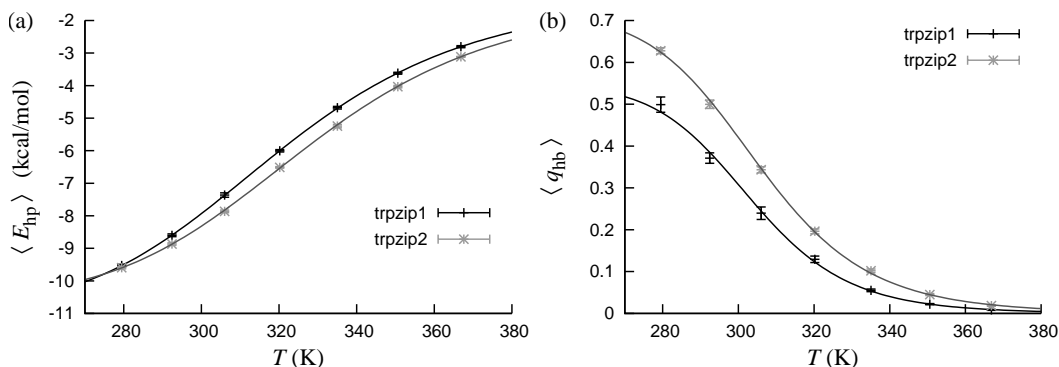


Figure 6: Trpzip1 and trpzip2. (a) Hydrophobicity energy E_{hp} against temperature. The lines are two-state fits ($T_m = 319.7 \pm 0.2$ K and $\Delta E = 7.9 \pm 0.1$ kcal/mol for trpzip1; $T_m = 327.1 \pm 0.8$ K and $\Delta E = 8.3 \pm 0.4$ kcal/mol for trpzip2). (b) Native-ness q_{hb} against temperature. The lines are two-state fits ($T_m = 303.2 \pm 1.8$ K and $\Delta E = 14.1 \pm 0.5$ kcal/mol for trpzip1; $T_m = 305.0 \pm 1.1$ K and $\Delta E = 12.6 \pm 0.3$ kcal/mol for trpzip2).

The β -hairpins trpzip1 and trpzip2. The 12-residue trpzip1 and trpzip2 are designed β -hairpins, each containing two tryptophans per β -strand (52). The only difference between the two sequences is a transposition of an asparagine and a glycine in the hairpin turn. CD measurements suggest that trpzip1 and trpzip2 are remarkably stable for their size, with T_m values of 323 K and 345 K, respectively (52). A complementary trpzip2 study, using both experimental and computational methods, found T_m values to be strongly probe-dependent (53).

Figure 5 shows our melting curves for these peptides, based on the observables E_{hp} and q_{hb} . The E_{hp} -based T_m values are 319.7 ± 0.2 K and 327.1 ± 0.8 K for trpzip1 and trpzip2, respectively. Using q_{hb} data instead, we find $T_m = 303.2 \pm 1.1$ K for trpzip1 and $T_m = 305.0 \pm 1.1$ K for trpzip2.

Like for the other β -hairpins discussed earlier, our q_{hb} -based folded populations are low compared to estimates based on CD data, whereas those based on E_{hp} are much closer to experimental data. For trpzip2, the agreement is not perfect but acceptable, given that T_m has been found to be strongly probe-dependent for this peptide (53).

Three-stranded β -sheets: betanova, LLM and beta3s. Betanova (54), the betanova triple mutant LLM (55) and beta3s (56) are designed 20-residue peptides forming three-stranded β -sheets. All the three peptides are marginally stable.

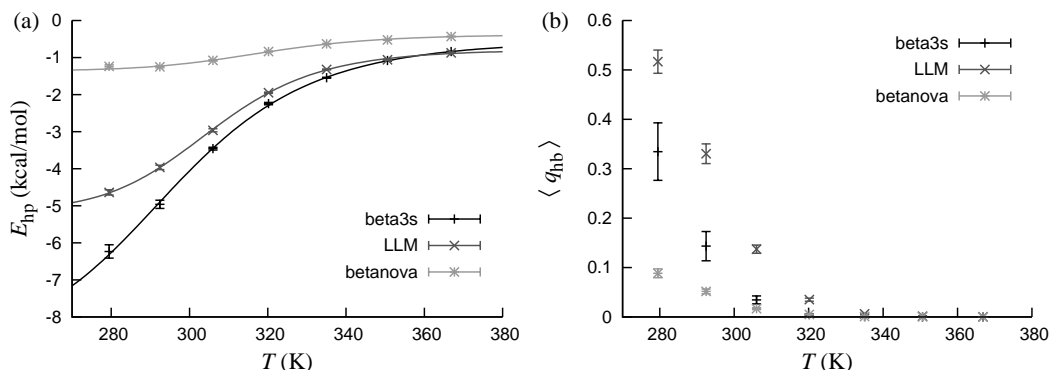


Figure 7: Betanova, LLM and beta3s. (a) Hydrophobicity energy E_{hp} against temperature. The lines are two-state fits ($T_m = 318.8 \pm 2.5$ K and $\Delta E = 13.3 \pm 2.1$ kcal/mol for betanova; $T_m = 305.6 \pm 1.7$ K and $\Delta E = 13.4 \pm 1.0$ kcal/mol for LLM; $T_m = 295.7 \pm 3.1$ K and $\Delta E = 9.7 \pm 0.5$ kcal/mol for beta3s). (b) Nativeness q_{hb} against temperature. Two-state fits were not possible.

NMR studies suggest that the folded population at 283 K is 0.09 for betanova (55), 0.36 for LLM (55), and 0.13–0.31 for beta3s (56).

Figure 6 shows our E_{hp} and q_{hb} data for these peptides. From the q_{hb} data, T_m values cannot be extracted, because the stability of the peptides is too low. At 283 K, the q_{hb} -based folded populations are 0.08, 0.47, 0.28 for betanova, LLM and beta3s, respectively, in good agreement with the experimental results. Fits to E_{hp} data can be performed. The obtained T_m values are 318.8 ± 2.5 K, 305.6 ± 1.7 K and 295.7 ± 3.1 K for betanova, LLM and beta3s, respectively.

These E_{hp} -based T_m values are high compared to the experimentally determined folded populations, especially for betanova. Note that betanova has a very low hydrophobicity. The correlation between E_{hp} and folding status is therefore likely to be weak for this peptide.

In contrast to the E_{hp} -based folded populations, those based on q_{hb} agree quite well with experimental data. In this respect, the situation is the opposite to what we found for the β -hairpins studied above. A possible reason for this difference is discussed below.

AB zipper. The AB zipper is a designed heterodimeric leucine zipper, composed of an acidic A chain and a basic B chain, each with 30 residues (57). The dimer structure has been characterized by NMR, and a melting temperature of ~ 340 K was estimated by CD measurements (at neutral pH) (57).

The lowest energy state seen in our simulations is a conformation in which pRMSD calculated over backbone atoms of all residues in both chains is ~ 2.7 Å. In this structure, the bRMSD (all residues) of the individual chains A and B to their counterparts in the PDB structure are ~ 2.5 Å and ~ 2.4 Å, respectively. Unlike for the other systems described in this article, the boundary conditions have a non-trivial role for this dimeric system. A proper discussion of periodicity, concentration and temperature dependence of this system is beyond the scope of this article. In Figure 7a, we show the energy landscape, i.e., the mean energy as a function of two order parameters for this system. The X-axis shows the measure pRMSD described earlier. The Y-axis represents the sum of the backbone RMSD of the individual chains. pRMSD can be very large even if the sum of bRMSDs is small: the two chains can be folded without making the proper inter-chain contacts. Indeed, the figure shows that the major energy gradients are along the Y-axis, showing that it is energetically favorable for both chains to fold to their respective helical states. The correct dimeric native state is energetically more favorable by ~ 20 kcal/mol compared to two folded helices without proper inter-chain contacts. This is seen more clearly in Figure 7b, where we plot the average energy as a function of pRMSD for states with two folded chains. We also simulated the two chains A and B of the dimer in isolation. Both chains folded to their native helical conformations. The melting temperatures estimated based on helix content for chains A and B are 314 K and 313 K, respectively. As indicated above, for the dimer, thermodynamic parameters like T_m cannot be directly estimated from the present simulations.

Top7-CFr. Top7-CFr, the C-terminal fragment of the designed 93-residue α/β -protein Top7 (58), is the most complex of all molecules studied here. It has both α -helix and β -strand secondary structure elements, and highly non-local hydrogen bonds between the N- and C-terminal strands. CFr is known to form extremely stable homodimers, which retain their secondary structure till very high temperatures like 371 K and high concentrations of denaturants (59).

In (13; 14), an earlier version of our model was used to study the folding of CFr. The simulations pointed to an unexpected folding mechanism. The N-terminal strand initially folds as a non-native continuation of the adjoining α -helix. After the other secondary structure elements form and diffuse to an approximately correct tertiary organization, the non-native extension of the helix unfolds and frees the N-terminal residues. These residues then attach to an ex-

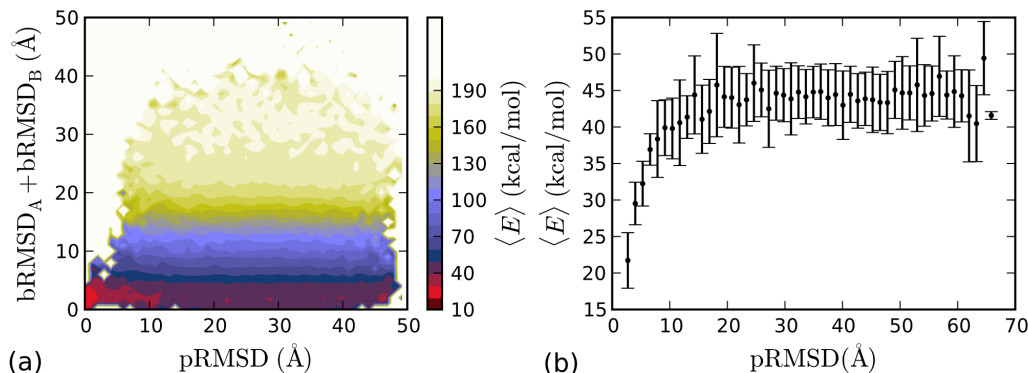


Figure 8: The heterodimeric AB zipper. (a) Mean energy as a function of pRMSD over both chains and the sum of individual bRMSDs. The direction of the energy gradients implies that a system with two folded monomers is energetically favorable compared to unfolded monomers. The proper dimeric form is the area closest to the origin, and has a lower energy. (b) Mean energy of all states in which both chains have bRMSD < 5 Å, shown as a function of the dimer RMSD measure pRMSD.

isting β -hairpin to complete the three-stranded β -sheet of the native structure. Premature fastening of the chain ends in β -sheet contacts puts the molecule in a deep local energy minimum, in which the folding and proper arrangement of the other secondary structure elements is hampered by large steric barriers. The above “caching” mechanism, spontaneously emerging in the simulations, accelerates folding by helping the molecule avoid such local minima.

The folding properties of CFr, including the above mentioned caching mechanism, are preserved under the current modifications of the interaction potential. The center of the native free-energy minimum shifts from bRMSD (all residues) of 1.7 Å as reported in (13) to about 2.2 Å. This state remains the minimum energy state, although the new energy function changes the energy ordering of the other low energy states. The runs made for this study (see Table 6) found 22 independent folding events. The free-energy landscape observed in the simulations is rather complex with a plethora of deep local minima sharing one or more secondary structure elements with the native structure. They differ in the registry and ordering of strands and the length of the helix. Longer runs are required for the MC simulations to correctly weight these different minima. Temperature dependence of the properties of CFr can therefore not be reliably obtained from these runs.

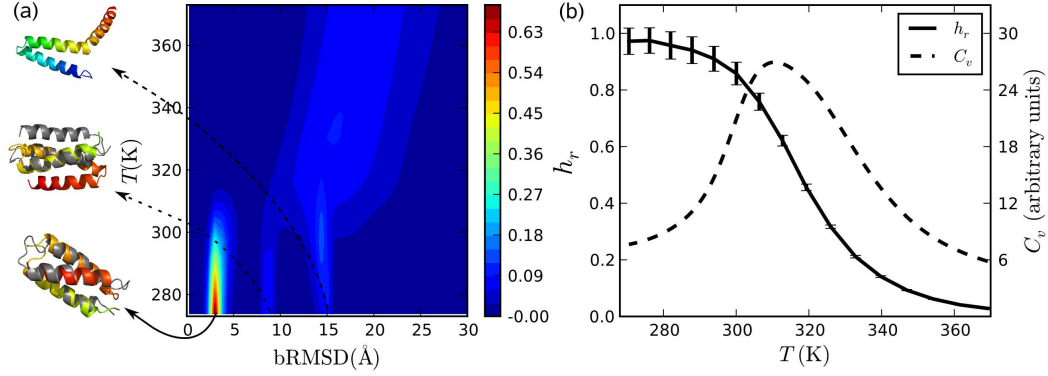


Figure 9: The three-helix-bundle protein GS- α_3 W. (a) Variation of histogram of bRMSD with temperature. At high temperatures, there is a broad distribution of bRMSD with values > 10 Å. At lower temperatures there are three clearly separated clusters. Representative structures from these clusters are also shown (color) aligned with the native structure (gray). (b) Temperature dependence of specific heat, C_v , and the ratio h_r of the observed helix content and the helix content of the native structure.

We note that the simulations ran on twice as many processors but were only about one sixth the length of those used for (13), in which 15 independent folding events were found. The improved efficiency is partly due to the changes in the energy function presented here, and partly due to the optimization of the parallel tempering described in (26).

GS- α_3 W. GS- α_3 W is a designed three-helix-bundle protein with 67 residues (60), whose structure was characterized by NMR (61). The stability was estimated to be 4.6 kcal/mol in aqueous solution at 298 K, based on CD data (60).

It turns out that this protein is very easy to fold with our model. Our results are based on extensive sampling of the conformation space with $64 \times 3.5 \times 10^9$ Monte Carlo updates, resulting in about 800 independent folding events to the native state. For this estimate, structures with bRMSD (all residues) under 5 Å were taken to be in the native minimum (see Figure 8 for justification). Two visits to the native state were considered statistically independent (i) if they occurred in independent Markov chains, or (ii) if the two visits to the native state were separated by at least one visit to the highest temperature in the simulation. For the entire run, we spent about 10 days of computing time on 64 AMD Opteron processors running at 2.0 GHz.

In Figure 8a, we show how the probabilities for structures with different bRMSD vary with temperature in the simulations. Clearly, the protein makes a transition from a rather continuous distribution of bRMSD at high temperatures to a distribution dominated by three well separated clusters. Analysis of the structures at the lower temperatures shows that all three free-energy minima consist almost exclusively of structures with all three helices of GS- α_3 W formed. The plot of the ratio of the observed helix content and the helix content of the native state, shown in Figure 8b, further supports this idea. The average value of this ratio approaches 1 as the temperature decreases below 300 K. The specific heat curve, also shown in Figure 8b, indicates that the formation of these structures correlates with the steepest change in energy.

The cluster with a center at bRMSD ~ 3 Å dominates at the lowest temperatures. The structures contributing to the cluster with ~ 8 – 9 Å bRMSD superficially look like well folded three-helix bundles. But as illustrated in the figure, the arrangement of the helices is topologically distinct from the native arrangement. The cluster seen at larger bRMSD values is broader and consists of a host of structures in which two of the helices make a helical hairpin, but the third helix is not bound to it. The unbound helix could be at either side of the chain.

According to our model therefore, the population at the lowest temperatures consists of $\sim 80\%$ genuinely native structures, $\sim 10\%$ three-helix bundles with wrong topology, and $\sim 10\%$ other structures with as much helix content as the native state. In order to experimentally determine the true folded population of the protein, the experimental probe must be able to distinguish the native fold from the other helix rich structures described here.

DISCUSSION

The model presented here is intrinsically fast compared to many other all-atom models, because all interactions are short range. By exploiting this property and using efficient MC techniques, it is possible to achieve a high sampling efficiency. We could, for example, generate more than 800 independent folding events for the 67-residue GS- α_3 W. The speed of the simulations thus permits statistically accurate studies of the global free-energy landscape of peptides and small proteins.

In developing this potential, a set of 17 peptides with 10–37 residues was studied. The peptides were added to this set one at a time. To fold a new sequence

sometimes required fine-tuning of the potential, sometimes not. A change was accepted only after testing the new potential on all previous sequences in the set. In its final form, the model folds all 17 sequences to structures similar to their experimental structures, for one and the same choice of potential parameters.

Also important is the stability of the peptides. A small polypeptide chain is unlikely to be a clear two-state folder, and therefore its apparent folded population will generally depend on the observable studied. For β -sheet peptides, we used the hydrophobicity energy E_{hp} and the hydrogen bond-based nativeness measure q_{hb} to monitor the melting behavior. The extracted T_{m} values indeed showed a clear probe dependence; the E_{hp} -based value was always larger than that based on q_{hb} . For the β -hairpins studied, we found a good overall agreement between our E_{hp} -based results and experimental data. For the three-stranded β -sheets, instead, the q_{hb} results agreed best with experimental data. The reason for this difference is unclear. One contributing factor could be that interactions between aromatic residues play a more important role for the β -hairpins studied here than for the three-stranded β -sheets. These interactions may influence spectroscopic signals and are part of E_{hp} . Probe-dependent T_{m} values have also been obtained experimentally, for example, for trpzip2 (53).

The probe dependence makes the comparison with experimental data less straightforward. Nevertheless, the results presented clearly show that the model captures many experimentally observed stability differences. In particular, among related peptides, the calculated order of increasing thermal stability generally agrees with the experimental order, independent of which of our observables we use.

It is encouraging that the model is able to fold these 17 sequences. However, there is no existing model that will fold all peptides, and our model is no exception. Two sequences that we unsuccessfully tried to fold are the β -hairpins trpzip4 and U_{16} , both with 16 residues. Trpzip4 is a triple mutant of GB1p with four tryptophans (52). For trpzip4, our minimum energy state actually corresponded to the NMR-derived native state (52), but the population of this state remained low at the lowest temperature studied ($\sim 14\%$ at 279 K, as opposed to an estimated T_{m} of 343 K in experiments (52)). U_{16} is derived from the N-terminal β -hairpin of ubiquitin (62). It has a shortened turn and has been found to form a β -hairpin with non-native registry (62). In our simulations, this state was only weakly populated ($\sim 8\%$ at 279 K, as opposed to an estimated $\sim 80\%$ at 288 K (62)). Instead, the main free-energy minima corresponded to the two

β -hairpin states with the registry of native ubiquitin, one with native hydrogen bonds and the other with the complementary set of hydrogen bonds.

Our calibration of the potential relies on experimental data with non-negligible uncertainties, on a limited number of peptides. It is not evident that this potential will be useful for larger polypeptide chains. Therefore, as a proof-of-principle test, we also studied three larger systems, with very good results. Our simulations showed that, without having to adjust any parameter, the model folds these sequences to structures consistent with experimental data. Having verified this, it would be interesting to use the model to investigate the mechanisms by which these systems self-assemble, but such an analysis is beyond the scope of this article. The main purpose of our present study of these systems was to demonstrate the viability of our calibration approach.

The potential can be further constrained by confronting it with more accurate experimental data and data on new sequences. The challenge in this process is to ensure backward compatibility — new constraints should be met without sacrificing properties already achieved.

CONCLUSION

We have described and tested an implicit solvent all-atom model for protein simulations. The model is computationally fast and yet able to capture structural and thermodynamic properties of a diverse set of sequences. Its computational efficiency greatly facilitates the study of folding and aggregation problems that require exploration of the full free-energy landscape. A program package, called PROFASI (28), for single- and multi-chain simulations with this model is freely available to academic users.

Acknowledgements. We thank Stefan Wallin for suggestions on the manuscript. This work was in part supported by the Swedish Research Council. The simulations of the larger systems were performed at the John von Neumann Institute for Computing (NIC), Research Center Jülich, Germany.

REFERENCES

1. Uversky VN: *Protein Sci.* 2002, **11**:739–756.
2. Dyson HJ, Wright PE: *Nat. Rev. Mol. Cell Biol.* 2005, **6**:197–208.

3. Yoda T, Sugita Y, Okamoto Y: *Chem. Phys.* 2004, **307**:269–283.
4. Shell MS, Ritterson R, Dill KA: *J. Phys. Chem.* 2008, **B 112**:6878–6886.
5. Irbäck A, Samuelsson B, Sjunnesson F, Wallin S: *Biophys. J.* 2003, **85**:1466–1473.
6. Irbäck A, Mohanty S: *Biophys. J.* 2005, **88**:1560–1569.
7. Cheon M, Chang I, Mohanty S, Luheshi LM, Dobson CM, Vendruscolo M, Favrin G: *PLoS Comput. Biol.* 2007, **3**:e173.
8. Irbäck A, Mitternacht S: *Proteins* 2008, **71**:207–214.
9. Li D, Mohanty S, Irbäck A, Huo S: *PLoS Comput. Biol.* 2008, **4**:e1000238.
10. Irbäck A, Mitternacht S, Mohanty S: *Proc. Natl. Acad. Sci. USA* 2005, **102**:13427–13432.
11. Mitternacht S, Luccioli S, Torcini A, Imparato A, Irbäck A: *Biophys. J.* 2009, **96**:429–441.
12. Mohanty S, Hansmann UHE: *Biophys. J.* 2006, **91**:3573–3578.
13. Mohanty S, Meinke JH, Zimmermann O, Hansmann UHE: *Proc. Natl. Acad. Sci. USA* 2008, **105**:8004–8007.
14. Mohanty S, Hansmann UHE: *J. Phys. Chem.* 2008, **B 112**:15134–15139.
15. Ponder JW, Case DA: *Adv. Protein Chem.* 2003, **66**:27–85.
16. Hubner IA, Deeds EJ, Shakhnovich EI: *Proc. Natl. Acad. Sci. USA* 2005, **102**:18914–18919.
17. Herges T, Wenzel W: *Phys. Rev. Lett.* 2005, **94**:018101.
18. Ding F, Tsao D, Nie H, Dokholyan NV: *Structure* 2008, **16**:1010–1018.
19. Hovmöller S, Zhou T, Ohlsson T: *Acta Cryst.* 2002, **D 58**:768–776.
20. Miyazawa S, Jernigan RL: *J. Mol. Biol.* 1996, **256**:623–644.
21. Li H, Tang C, Wingreen NS: *Phys. Rev. Lett.* 1997, **79**:765–768.
22. Lyubartsev AP, Martsinovski AA, Shevkunov SV, Vorontsov-Velyaminov PN: *J. Chem. Phys.* 1992, **96**:1776–1783.
23. Marinari E, Parisi G: *Europhys. Lett.* 1992, **19**:451–458.
24. Swendsen RH, Wang JS: *Phys. Rev. Lett.* 1986, **57**:2607–2609.
25. Hukushima K, Nemoto K: *J. Phys. Soc. (Jap)* 1996, **65**:1604–1608.
26. Meinke J, Mohanty S, Nadler W: *Manuscript in preparation*, 2009.
27. Favrin G, Irbäck A, Sjunnesson F: *J. Chem. Phys.* 2001, **114**:8154–8158.
28. Irbäck A, Mohanty S: *J. Comput. Chem.* 2006, **27**:1548–1555.
29. García AE, Sanbonmatsu KY: *Proc. Natl. Acad. Sci. USA* 2002, **99**:2782–2787.
30. Miller RG: *Biometrika* 1974, **61**:1–15.
31. DeLano WL: *San Carlos, CA: DeLano Scientific* 2002.
32. Gnanakaran S, Nymeyer H, Portman J, Sanbonmatsu KY, García AE: *Curr. Opin. Struct. Biol.* 2003, **13**:168–174.
33. Meinke J, Hansmann UHE: *Submitted manuscript*, 2009.

34. Neidigh JW, Fesinmeyer RM, Andersen NH: *Nat. Struct. Biol.* 2002, **9**:425–430.
35. Liu Y, Liu Z, Androphy E, Chen J, Baleja JD: *Biochemistry* 2004, **43**:7421–7431.
36. Qiu L, Pabit SA, Roitberg AE, Hagen SJ: *J. Am. Chem. Soc.* 2002, **124**:12952–12953.
37. Streicher WW, Makhatadze GI: *Biochemistry* 2007, **46**:2876–2880.
38. Bierzynski A, Kim PS, Baldwin RL: *Proc. Natl. Acad. Sci. USA* 1982, **79**:2470–2474.
39. Scholtz J, Barrick D, York E, Stewart J, Baldwin R: *Proc. Natl. Acad. Sci. USA* 1995, **92**:185–189.
40. Shoemaker KR, Kim PS, York EJ, Stewart JM, Baldwin RL: *Nature* 1987, **326**:563–567.
41. Lockhart DJ, Kim PS: *Science* 1992, **257**:947–951.
42. Lockhart DJ, Kim PS: *Science* 1993, **260**:198–202.
43. Thompson PA, Eaton WA, Hofrichter J: *Biochemistry* 1997, **36**:9200–9210.
44. Williams S, Causgrove TP, Gilmanshin R, Fang KS, Callender RH, Woodruff WH, Dyer RB: *Biochemistry* 1996, **35**:691–697.
45. Chakrabartty A, Ananthanarayanan VS, Hew CL: *J. Biol. Chem.* 1989, **264**:11307–11312.
46. Steinmetz MO, Jelesarov I, Matousek WM, Honnappa S, Jahnke WA, Missimer JH, Frank S, Alexandrescu AT, Kammerer RA: *Proc. Natl. Acad. Sci. USA* 2007, **104**:7062–7067.
47. Honda S, Yamasaki K, Sawada Y, Morii H: *Structure* 2004, **12**:1507–1518.
48. Pastor MT, López de la Paz M, Lacroix E, Serrano L, Pérez-Payá E: *Proc. Natl. Acad. Sci. USA* 2002, **99**:614–619.
49. Blanco F, Rivas G, Serrano L: *Nat. Struct. Biol.* 1994, **1**:584–590.
50. Fesinmeyer RM, Hudson FM, Andersen NH: *J. Am. Chem. Soc.* 2004, **126**:7238–7243.
51. Muñoz V, Thompson PA, Hofrichter J, Eaton WA: *Nature* 1997, **390**:196–199.
52. Cochran AG, Skelton NJ, Starovasnik MA: *Proc. Natl. Acad. Sci. USA* 2001, **98**:5578–5583.
53. Yang WY, Pitera JW, Swope WC, Gruebele M: *J. Mol. Biol.* 2004, **336**:241–251.
54. Kortemme T, Ramírez-Alvarado M, Serrano L: *Science* 1998, **281**:253–256.
55. López de la Paz M, Lacroix E, Ramírez-Alvarado M, Serrano L: *J. Mol. Biol.* 2001, **312**:229–246.
56. de Alba E, Santorio J, Rico M, Jimenez MA: *Protein Sci.* 1999, **8**:854–865.
57. Marti DN, Bosshard HR: *Biochemistry* 2004, **43**:12436–12447.
58. Kuhlman B, Dantas G, Ireton GC, Varani G, Stoddard BL, Baker D: *Science* 2003, **302**:1364.
59. Dantas G, Watters AL, Lunde BM, Eletr ZM, Isern NG, Roseman T, Lipfert J, Doniach S, Tompa M, Kuhlman B, Stoddard BL, Varani G, Baker D: *J. Mol. Biol.* 2006, **362**:1004–1024.
60. Johansson JS, Gibney BR, Skalicky JJ, Wand AJ, Dutton PL: *J. Am. Chem. Soc.* 1998,

120:3881–3886.

61. Dai QH, Thomas C, Fuentes EJ, Blomberg MRA, Dutton PL, Wand AJ: *J. Am. Chem. Soc.* 2002, **124**:10952–10953.
62. Jourdan M, Griffiths-Jones SR, Searle MS: *Eur. Biophys. J.* 2000, **267**:3539–3548.